NEAR WALL FLOW OVER URBAN-LIKE ROUGHNESS

HONG CHENG[1] and IAN P. CASTRO[2]
[1]*EnFlo, School of Engineering, University of Surrey, Guildford GU2 7XH, U.K.;* [2]*School of Engineering Sciences, University of Southampton, Southampton SO17 1BJ, U.K.*

(Received in final form 7 November 2001)

Abstract. In this study, comprehensive measurements over a number of urban-type surfaces with the same area density of 25% have been performed in a wind tunnel. The experiments were conducted at a free stream velocity of 10 m s^{-1} and the main instrumentation was 120° x-wire anemometry, but measurement accuracy was checked using laser Doppler anemometry. The results have confirmed the strong three-dimensionality of the turbulent flow in the roughness sublayer and the depths of the inertial sublayer (log-law region) and roughness sublayer for each surface have been determined. Spatial averaging has been used to remove the variability of the flow in the roughness sublayer due to individual obstacles and it is shown that the spatially averaged mean velocity in the inertial sublayer and roughness sublayer can, together, be described by a single log-law with a mean zero-plane displacement and roughness length for the surface, provided that the proper surface stress is known. The spatially averaged shear stresses in the inertial sublayer and roughness sublayer are compared with the surface stress deduced from form drag measurements on the roughness elements themselves.

The dispersive stress arising from the spatial inhomogeneity in the mean flow profiles was deduced from the data and is shown to be negligible compared with the usual Reynolds stresses in the roughness sublayer. Comparisons have been made between a homogeneous (regular element array) surface and one consisting of random height elements of the same total volume. Although the upper limits of the inertial sublayer for both surfaces were almost identical at equivalent fetch, the roughness sublayer was much thicker for the random surface than for the uniform surface, the friction velocity and the roughness length were significantly larger and the 'roughness efficiency' was greater. It is argued that the inertial sublayer may not exist at all in some of the more extreme rough urban areas. These results will provide fundamental information for modelling urban air quality and forecasting urban wind climates.

Keywords: Form drag, Roughness sublayer, Spatial average, Urban random surface, Wind tunnel.

1. Introduction

The boundary layer over a rough surface is characterised by a surface layer, which can be subdivided into the inertial sublayer and roughness sublayer (Raupach et al., 1980, 1991). Within the inertial sublayer (hereafter denoted by IS) the vertical variation of the shear stress may be neglected and the wind direction is assumed to be constant with height. The vertical variation of the wind speed under neutral stability can be described by the usual logarithmic law:

$$U = \frac{u_*}{k} \ln\left(\frac{z-d}{z_0}\right) \tag{1}$$

Boundary-Layer Meteorology **104:** 229–259, 2002.

where k is the von Karman constant, taken here as 0.4. The friction velocity u_*, which represents the effect of wind stress τ_0 on the ground, is defined by $u_* = (\tau_0/\rho)^{0.5}$, where ρ is the air density. z_0 is the roughness length and d is the zero-plane displacement. Stull (1988) pointed out that, for fully developed (and fully rough) flow, z_0 and d are surface properties determined by roughness geometry and independent of wind speed and stability. In practical wind-tunnel simulations and some field measurements, the friction velocity u_* is normally deduced from the measured shear stress profile in the inertial sublayer; z_0 and d are then determined by fitting the mean velocity measurements in the inertial sublayer to the above equation using u_* as the slope. Here it is emphasised that the roughness length can only be defined when there is a logarithmic velocity profile.

The region of the flow beneath the inertial sublayer is known as the roughness sublayer (hereafter denoted by RS), within which the flow is strongly influenced by the individual roughness elements and is therefore not spatially homogeneous. The top of the RS is often said to be at 2 to 5 times the height of the roughness element measured from the ground, but no systematic studies are available in the literature. For urban surfaces, the lowest part of the RS is called the urban canopy layer (UCL) and has a depth equal to the mean building height, h, or (perhaps) the zero-plane displacement height, d (Rotach, 1993a). The few extant studies on the urban canopy layer have indicated that the mean velocity within this layer obeys an exponential decay law (Plate, 1982; Macdonald et al., 2000), but the exponential wind profile in the UCL is not as well founded physically as the logarithmic law in the IS. Very little is known about the depths of the various layers over most surfaces.

Over the last few decades a large number of field and wind-tunnel studies have steadily advanced our knowledge of turbulence over vegetation surfaces. A detailed summary can be found in Raupach et al. (1996). Compared with rural areas, the boundary layer over urban surfaces is in general not well understood, due to its complex nature and the inevitable experimental difficulties associated with regions of high turbulence intensity (Roth, 2000). The dominant features of urban surfaces are the very heterogeneous roughness elements (buildings and other man-made structures) that are relatively large and usually irregularly 'arranged'. Currently numerical weather prediction models represent such urban areas in just the same way as less rough areas, i.e., assuming that an inertial sublayer and thus a logarithmic law exists and using some more or less appropriate roughness length z_0 and/or friction velocity u_*. Accurate determination of z_0 and u_* is thus crucial for the model and thus for forecasting the behaviour of urban wind and turbulence, even accepting the premise of the existence of the IS.

Over an urban area the roughness sublayer may extend to a significant height and the inertial sublayer then becomes squeezed between the RS and the outer layer. In addition, when the characteristics of the surface change, the vertical extent of the urban inertial sublayer is also affected by the development of an internal boundary layer. An earlier study on step changes in roughness (Cheng and Castro,

2002) showed explicitly what might intuitively be anticipated – that the growing equilibrium layer has first to encompass the roughness sublayer before any thickness of inertial sublayer can be developed. Therefore in some practical cases, like flows across urban environments where the underlying surface may constantly change, it is possible that a representative inertial sublayer for the underlying surface does not exist at all. This makes the determination of the roughness length from point mean velocity measurements impossible; indeed, it raises the question as to whether z_0 is actually an appropriate scale for such flows.

The depth of the roughness sublayer is a subject of on-going debate (Roth and Oke, 1993) and there is little information available on characterisation of the flow within the RS. On the basis of field observations over forests (Garratt, 1980) and cities (Rotach, 1993a, 1993b, 1995) as well as measurements taken in wind tunnels (e.g., Mulhearn and Finnigan, 1978; Raupach et al., 1980), it seems likely that, like the roughness length z_0, the depth of the roughness sublayer is dependent on the geometrical properties of the surface such as the shape and size of the obstacles, their layout and the consequent area density. Different RS thicknesses would be expected over different types of terrain. Because of (typically) height limitations of measurement towers, meteorological data used to derive u_*, z_0 and d are often actually obtained in the roughness sublayer rather than within the IS, which is likely to be inappropriate for overall parameterisation.

The flow in the inertial sublayer is known to be logarithmic (and perhaps is exponential within the UCL), but no attempts have been made to determine a general vertical profile within the RS. MacDonald et al. (2000) and MacDonald (2000) considered lateral (i.e., spanwise) averages within and just above the urban canopy in cube arrays, but they did not extend the idea to develop a spatially averaged vertical profile. Because the flow within the roughness sublayer is inherently three dimensional, taking measurements at only one vertical line within a limited vertical range, as done in some field measurements, may not really lead to a satisfactory description of the flow. However, full spatial averaging over (at least) one 'repeating-unit' of a uniform array will lead to a 'representative' profile within the RS, which could then be regarded as horizontally homogeneous on scales larger than that unit. It is not immediately obvious whether such a spatially averaged profile would be logarithmic (following the IS above or not) although evidence from the much larger 'roughness' formed by periodic arrays of hills suggests that this might be so (Wood and Mason, 1993). The first attempt at spatially averaging the flow over a unit was probably made by Raupach et al. (1986), who studied the turbulent structure over and within a model plant canopy; they found that the averaged velocity profiles in the RS was not logarithmic over plant canopies.

The main objective of this study is to investigate the characteristics of the turbulent flow in the surface layer in order to understand the process governing the exchange of momentum between the urban surface and the atmosphere and thus to provide a foundation for improving the current parameterisation of the surface flow. Because sources of pollutant are often situated within or close to the roughness

sublayer in urban environments, knowledge of the structure of the turbulence in the roughness sublayer is also essential for improving urban dispersion models, which strongly depend on the meteorological conditions. In this study, we will describe experiments over a number of simplified urban surfaces and attempt to determine (1) the nature of the spatially averaged flow within the roughness sublayer, (2) the depths of the inertial sublayer and the roughness sublayer for each roughness as well as the effect of wind direction on the depths of these layers, (3) the development of the IS and the RS with fetch, (4) the turbulence characteristics over urban surfaces and their spatial averages, and (5) surface parameterisation over these urban-like roughnesses.

2. Experimental Set-Up

2.1. WIND TUNNEL

Experiments were conducted in the EnFlo 'A' tunnel, which is a low speed open-circuit tunnel with a test section of 600 mm high, 900 mm wide and 4.5 m long. The free stream velocity in the wind tunnel was measured by a Pitot-static tube and all the measurements described here were carried out at a nominal free stream velocity of 10 m s^{-1}. The pressure gradient along the test section in the wind tunnel is negligible under the flow conditions investigated ($\frac{\nu}{\rho u_*^2}\frac{dp}{dx} < 0.001$). (x, y, z) are the streamwise, lateral and vertical coordinates, with the plane $z = 0$ being the top surface of the baseboard on which the roughness elements were located. Mean and fluctuating velocities will be denoted as (U, V, W) and (u, v, w) respectively. Time-averaged fluctuating quantities are denoted by overbars.

2.2. ROUGHNESS SURFACES

The roughness elements, chosen to represent idealised urban surfaces, were sharp-edged cubes and rectangular blocks. There were four rough surfaces involved in this study as schematically shown in Figure 1–3, and they are summarised in Table I.

For the 20-mm cube arrays (C20A and C20S) the elements were made from wood and glued onto five separate square baseboards (880 × 880 × 9 mm) in staggered pattern. For the 10-mm cube array (C10S) and the random array (RM10S) the elements were moulded (in an ABS material) into a square unit (80 × 80 × 2 mm) which contained 16 elements. Like the 20-mm cube arrays, these square units were then glued onto five baseboards (880 × 880 × 6 mm) in staggered pattern. Manufacturing restrictions meant that each of the four side walls of the elements was inwardly inclined at 1° to the vertical.

In designing the random array, it was recognised that actual urban areas have elements that are not only of random height and shape but also randomly spaced.

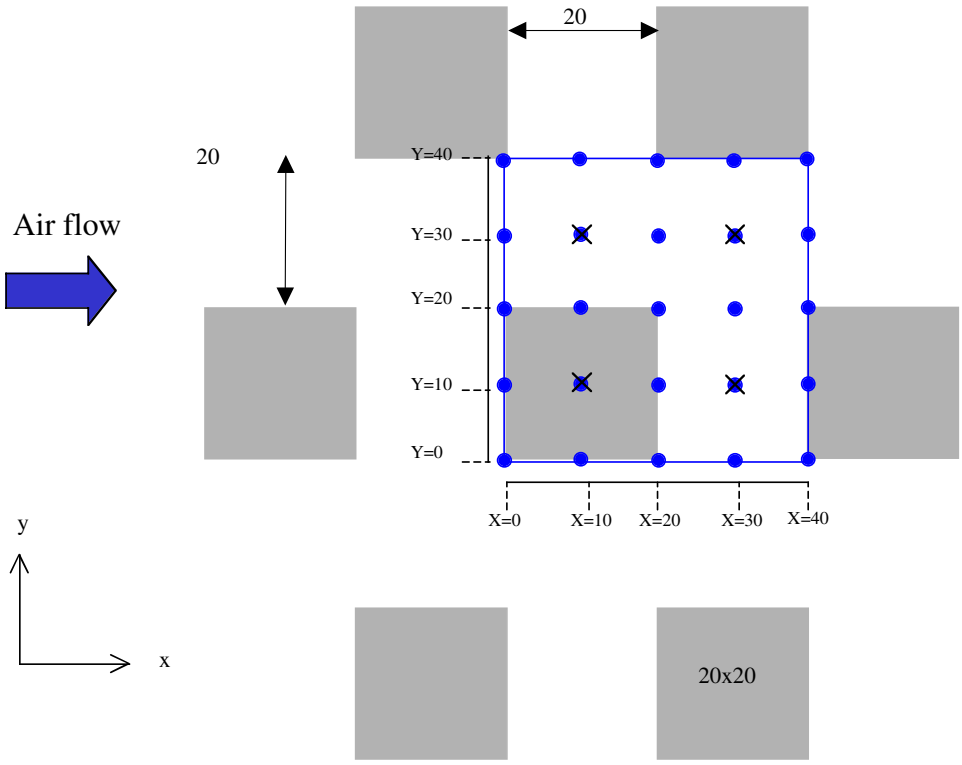

Figure 1. Schematic plan view for aligned cube array C20A.

TABLE I
Details of the roughness arrays.

Surface	C20A	C20S	C10S	RM10S
Pattern	Aligned	Staggered	Staggered	Staggered
Roughness element	Uniform cube	Uniform cube	Uniform cube	Random blocks
Element height (mm)	20	20	10	Normal distribution
Profiles in uw plane	25	4	4	64
Profiles in uv plane	4	4	4	None
Instrumentation	120° x-wire	120° x-wire and LDA	120° x-wire	120° x-wire
Unit size (mm × mm)	40 × 40	40 × 40	20 × 20	80 × 80
Area coverage density	25%	25%	25%	25%
Elements in a unit	1	1	1	16

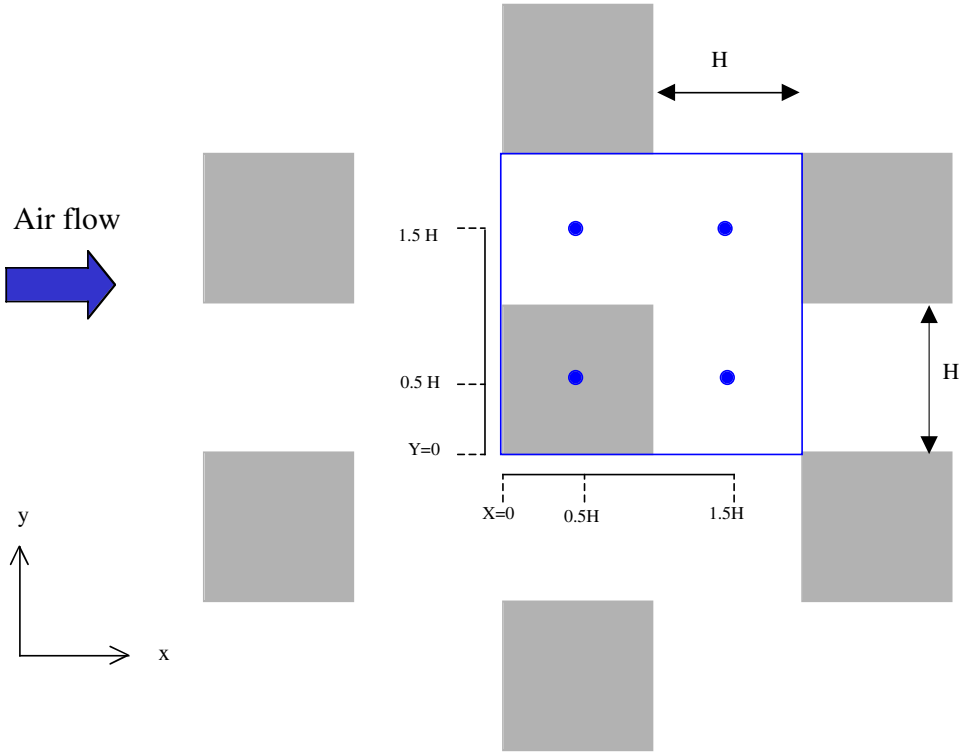

Figure 2. Schematic plan view for staggered cube arrays (C20S and C10S).

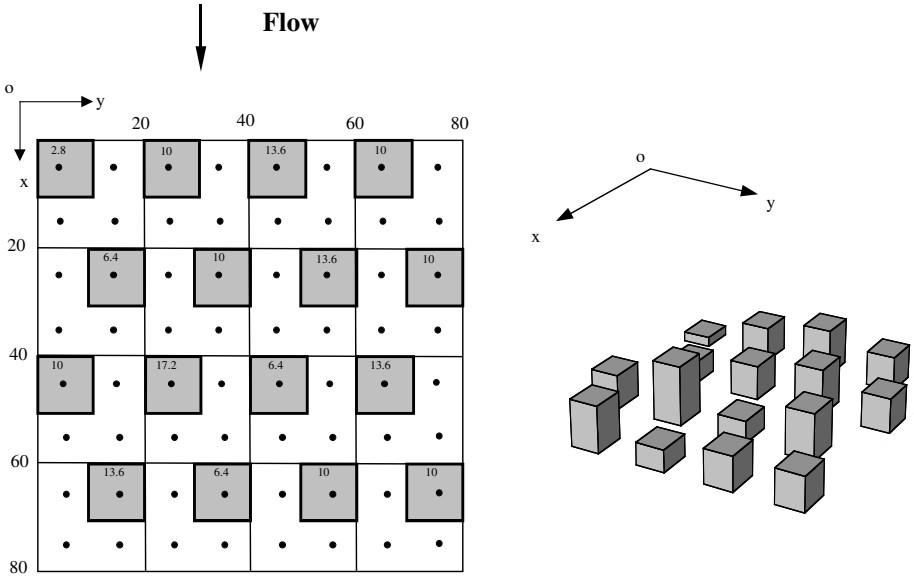

Figure 3. Schematic plan view and 3D view for staggered random arrays (RM10S). Dimensions in mm, with element heights indicated on the plan view.

The number of characterising variables is therefore impossibly large, even for a fixed total element volume within a given plan area. It was decided to begin our work on such arrays by restricting the randomness to height only, maintaining both the cross-sectional (square) shape and the staggered area density (25%). It was then necessary to decide on an appropriate size of 'repeating unit'; this needed to be large enough to allow a significant degree of variability in element height but small enough to prevent significant flow development (e.g., increase in boundary-layer depth) across it and to restrict the required vertical profiles for adequate spatial averaging to a manageable number. These considerations led to a choice of 80 mm $\times$ 80 mm as the size of the 'repeating unit' of the RM10S surface (80 mm was around one half of the expected boundary-layer thickness), on which were placed in regular staggered pattern sixteen 10-mm-square elements having five different heights chosen from a normal distribution with a mean and standard deviation of 10mm and 3mm respectively. Note that this ensured that the total element volume, as a percentage of the product of the repeating unit area and the mean element height, was identical to that of the regular 10-mm cube array (25%). Although the elements were arranged in a regular staggered pattern (just as for the C10S surface) the choice of which element (from the set of 16) should go in each position was also randomised. Schematic drawings for all the roughnesses studied here are shown in Figure 1–3; the vertical profile locations are indicated by dots.

All the surfaces, which had the same area coverage density of 25%, were so designed that by rotating each of the five baseboards by 90°, an aligned array could be obtained. In every case the roughness covered the entire floor of the wind tunnel and a ramp was positioned at the front of the first roughness board to provide a smooth transition between the contraction exit and the rough surface. For comparison purpose among different roughnesses most traverses were taken around the tunnel centre line and about 3 m downstream of the ramp. The boundary-layer thickness at the measurement location was defined as the height at which the velocity was 99% of the free stream velocity. Comparisons between aligned and staggered cube arrays, and between form drag measurements and direct shear stress measurements, were performed over the C20A and C20S surfaces, whereas comparisons between data for roughnesses having different size and shape elements were made over the C20S, C10S and RM10S arrays.

2.3. INSTRUMENTATION

Hot wire anemometry (HWA) was the main instrumentation used in this study. The signals from the bridges of a constant temperature system from Prosser Scientific Instruments (model 6100) were filtered and then digitised *via* a 16 bit A/D converter (ADC 488/8SA), which was operated by 'home-grown' virtual instruments written using LabView (from National Instruments) loaded on an Apple Macintosh computer. The probes were gold-plated tungsten wires with an active length of about 1 mm and the x-wires were nominally $\pm 60°$ to the mean flow direction

– i.e., the two wires had an included angle of 120°. This larger angle than the normal 90° (with standard ±45° wires) was used to minimise the errors arising from inadequate yaw response in highly turbulent flows; Perry et al. (1987) have shown that such probes yield significantly more accurate data above rough surfaces than can be obtained with standard x-wires. The probes were calibrated in the free stream against a pitot-static tube. Calibration checks were made in the free stream at the beginning and the end of each profile and if the difference between the mean velocity obtained from the x-wire probe and the pitot-static tube exceeded 1% the profile was rejected and calibration repeated. The detailed calibration and analysis procedures have been described elsewhere (Snyder and Castro, 2002). For all the measurements, corrections accounting for the cooling effects due to the third component of velocity and effective rectification caused by a hot wire's insensitivity to flow direction (Tutu and Chevray, 1975) have been applied to improve further the likely accuracy; all the results presented here are corrected data. A sampling frequency of 200 Hz and sampling time of 40 s was generally used at each measurement location.

An alternative solution to obtaining accurate measurements in the highly turbulent flows that occur in roughness sublayers of this sort is to use laser Doppler anemometry (LDA). As a check on the adequacy of the hot wire data some additional measurements were made using a dual beam LDA fibre-optic probe head fitted beneath the wind tunnel on a height gauge, so that the measurement position could be recorded. The beams were directed vertically through an optical window mounted in the tunnel floor and then reflected through 90° using an elliptical mirror in order to position the measurement volume horizontally and hence to measure the u and w components of the flow simultaneously. Figure 4 shows the set-up. One major limitation was that since the focal length of the beams was only 120 mm, the (fixed) distance from the probe to the mirror limited the maximum height above the roughness at which measurements could be obtained. Bubbles of fluid created by ultrasonic pulses in a hydrosonic seeding machine were used as tracer particles; these had a diameter of around 2 μm. The LDA was only used for the C20S array and the vertical profiles were taken in the region $26 < z < 45$ mm at the same locations and flow conditions as used in the hot wire experiments.

The spatially averaged and individual profiles of each quantity taken by the LDA and the 120° x-wire at the same locations were compared and it was found that the mean velocity from the 120° x-wire was generally slightly higher than that from the LDA. No obvious difference was detected in the profiles of $\overline{uw}$ and $\overline{w^2}$ from both measurement techniques (provided the x-wire data were corrected for high-turbulence effects); $\overline{u^2}$ from the 120° x-wire, however, was consistently larger than that from the LDA and the difference increased as the height decreased, reaching some 10% at the lowest elevations. The u_* values from both measurement techniques were almost identical (with less than 1% difference) and this, along with the small differences in mean velocity, led to a roughness length derived from the LDA some 20% higher than that from the x-wire data. Overall, these tests

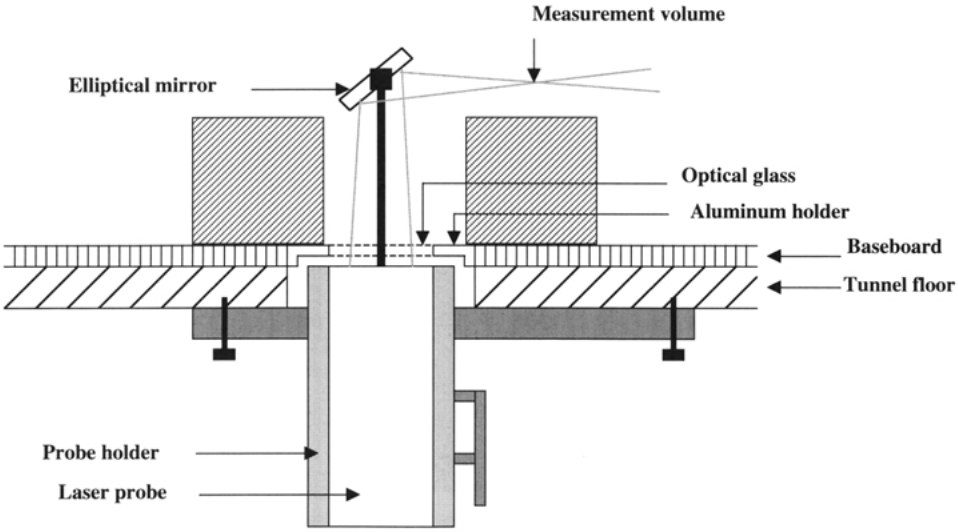

Figure 4. Laser Doppler Anemometry set-up in 'A' tunnel.

confirmed the adequacy of the 120° x-wire technique and, since the LDA was much less convenient to use, it was not employed for the majority of the work.

Form drag of the C20A and C20S surfaces was measured by replacing one of the wooden cube elements with a special brass cube located 2870 mm downstream of the ramp. This was fitted with 21 pressure taps (0.6 mm in diameter) located in different positions on both the front and back faces. Pressure distributions at 42 locations – on both faces, by rotating the cube through 180° – were obtained using a temperature controlled pressure transducer (Baratron) and a scani-valve, at three different free-stream velocities (10, 6 and 4 m s^{-1}). The static pressure from the pitot-static tube, which was located in the free-stream above the measurement position, was used as the reference pressure. For these pressure measurements, a sampling frequency of 50 Hz and a sampling time of 40 s at each point were used throughout.

3. Surface Friction Velocity from Form Drag Measurements

The surface shear stress can be estimated by measuring the form drag over a unit area (i.e., one horizontal square of side $2h$ containing just one element) and assuming that the viscous drag is negligible, which is considered very likely for the present 25% area-coverage rough surfaces. The drag force D of the flow on an individual cube was determined by integrating the pressure distribution over the front and back face of the cube and then using the relations:

$$D = \int_A (p_f - p_b) dA, \tag{2a}$$

TABLE II
Form drag measurements over C20A and C20S.

Surface	U_r (m s^{-1})	C_d (U at $z = h$)	C_d (U at $z = 1.5h$)	C_d ($U = U_r$)	$u_*(p)/U_r$	Re
C20S	10.15	1.071	0.201	0.042	0.0724	1.2×10^4
	6.14	1.020	0.192	0.040	0.0705	0.7×10^4
	4.03	1.071	0.201	0.042	0.0723	0.5×10^4
C20A	10.17	0.652	0.188	0.037	0.0679	1.2×10^4
	6.17	0.634	0.183	0.036	0.0666	0.7×10^4
	4.16	0.599	0.173	0.034	0.0656	0.5×10^4

$$C_d = \frac{2D}{\rho U_r^2 A}, \tag{2b}$$

$$\tau_p = \frac{D}{A_c}, \tag{2c}$$

$$u_*(p) = \sqrt{\frac{\tau_p}{\rho}}, \tag{2d}$$

where p_f and p_b are the pressures on the front and back faces respectively, A is the frontal area of the element, U_r is the free stream velocity, A_c is the unit (plan) area of the roughness surface ($4h^2$), τ_p is the shear stress due to the form drag, $u_*(p)$ is the friction velocity determined from the surface shear stress and ρ is the air density. C_d is the drag coefficient based on the free stream velocity. Alternatively, the drag coefficient can also be based on the spatially averaged mean velocity over a repeating area at, say, $z = h$ or 1.5 h, where h is the roughness element height. These could perhaps be considered more appropriate velocity scales than the free-stream value. Because the vertical profiles were only measured at one nominal free-stream velocity of 10 m s^{-1}, here (for the purpose of calculating the alternative reference velocities – which were below the measurement range) it is assumed that the value of u_*/U_r for each surface is independent of free-stream velocity in the range of 10 to 4 m s^{-1}. All the results for both staggered and aligned cube arrays are listed in Table II, in which the Reynolds number is based on the cube height and the free-stream velocity.

These results confirm that the form drag coefficient is only a weak function of the Reynolds number in the velocity range investigated. The C_d values are significantly smaller than that for an isolated sharp edged cube in a turbulent boundary layer at a similar Reynolds number (e.g., 1.18 as given by Modi and Deshpande, 2001), even when using a velocity in the RS as a reference, no doubt because of the sheltering effect of the surrounding cubes. Perhaps not surprisingly, the staggered arrays experience a higher drag force than the aligned cube array at the same flow

conditions, which is consistent with the greater degree of sheltering provided by upstream elements.

4. Profile Results and Discussion

4.1. 25-POINT-AVERAGE VS 4-POINT-AVERAGE OVER C20A SURFACE

The (fixed height) spatially averaged quantities are defined as follows:

$$\bar{U}_{sa} = \frac{1}{n}\sum_{i=1}^{n}\bar{U}_i, \tag{3a}$$

$$\overline{u^2}_{sa} = \frac{1}{n}\sum_{i=1}^{n}\overline{u^2}_i, \tag{3b}$$

$$\overline{v^2}_{sa} = \frac{1}{n}\sum_{i=1}^{n}\overline{v^2}_i, \tag{3c}$$

$$\overline{w^2}_{sa} = \frac{1}{n}\sum_{i=1}^{n}\overline{w^2}_i \tag{3d}$$

$$\overline{uw}_{sa} = \frac{1}{n}\sum_{i=1}^{n}\overline{uw}_i, \tag{3e}$$

where n is the number of profiles taken within a repeating area. Because of the nature of the flow in the roughness sublayer, to obtain representative spatially-averaged turbulent properties within this layer it is necessary to average a sufficiently large number of individual point measurements. Too great a number would obviously lead to a very time-consuming measurement programme and, for the aligned cube arrays, it was decided to obtain 25 vertical profiles, uniformly distributed in a unit area (40 $\times$ 40 mm) at the 'dot' locations shown in Figure 1. For each quantity (mean velocity and Reynolds stresses) the 25 values gathered at each height were averaged, leading to 25-point-average vertical profiles. These profiles were then compared with the corresponding averaged vertical profiles of each quantity obtained using just the four individual locations identified by the crosses shown in Figure 1. The results are illustrated in Figure 5. Apart from the shear stress at small z where the differences could nonetheless be within the experimental error in this particularly highly turbulent region, these two averaging methods essentially lead to very similar profiles. To save time, therefore, spatial averaging over the staggered cube arrays (C20S and C10S) was carried out using

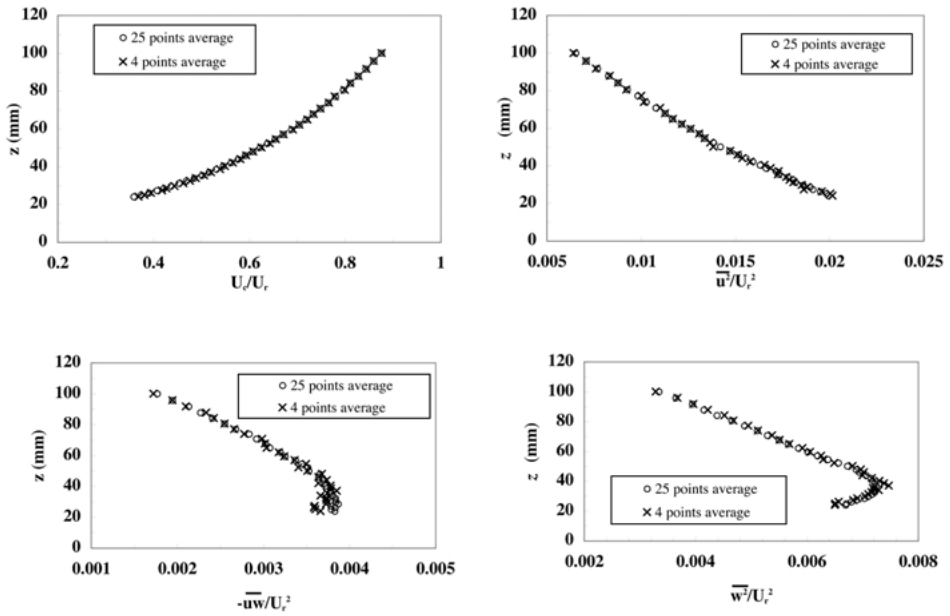

Figure 5. Comparison between 25 and 4 points averaged vertical profiles over aligned cube arrays (C20A).

only the four corresponding locations, but it should be emphasised that such a simplification may not be generally valid for other surfaces, particularly for more random and complex shaped roughness. It would certainly not be appropriate for the random surface and, in that case, 64 profiles were obtained at the locations indicated by the dots in Figure 3.

4.2. Depths of the IS and RS

The concepts of the inertial sublayer and roughness sublayer for rough wall boundary layers are not particularly new but, as stated earlier, there is little information available in the literature on how to define the depths of these layers. With increasing height the vertical profiles taken in different locations will eventually converge and it is this 'convergence height' that we define as the upper limit of the RS (and the lower limit of the IS). The IS is here defined as the region within which the vertical variation of the spatially averaged shear stress is confined to 5%. These definitions are somewhat arbitrary but alternative definitions do not lead to substantive changes in our major conclusions.

For the C20A roughness, the vertical profiles of the normal and shear stresses normalised using the free stream velocity are shown in Figure 6 for $z < 100$ mm. The shear stress data in the IS and the outer layer have a scatter within $\pm 7\%$ at most, which is typical for crossed hot wire measurements. However, the much lar-

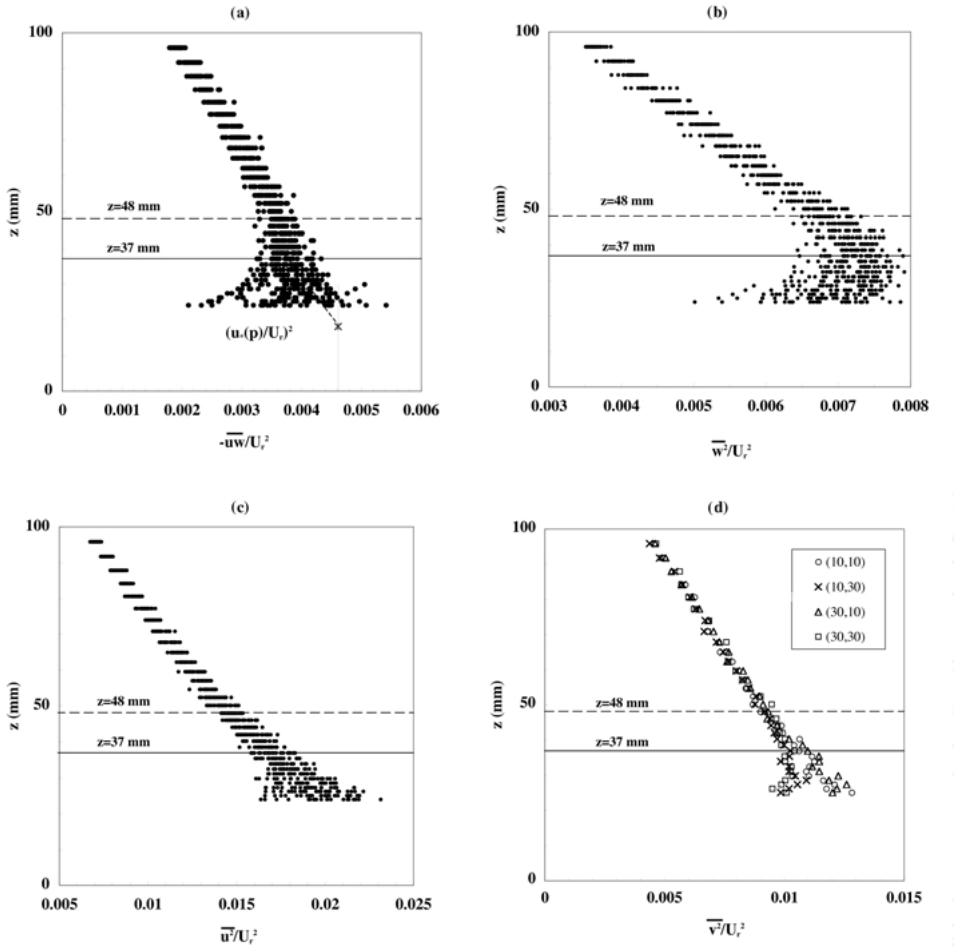

Figure 6. Vertical profiles over aligned cube arrays (C20A): (a) Shear stress; (b) vertical stress; (c) longitudinal stress; (d) lateral stress.

ger variability at lower heights is clearly a result of spatial inhomogeneities rather than experimental uncertainty. Within the roughness sublayer whether the shear stress increases, is constant or even decreases with height is entirely dependent on the profile's location. Examining all the shear stress profiles taken within a unit area for C20A in Figure 6a, it seems clear that the spatial homogeneity is established by about $z = 37$ mm, and above this height, a further change in shear stress limited to a fall of 5% suggests an upper limit to the inertial sublayer of about $z = 48$ mm. Figures 6a–6d indicate the IS and RS regions for the C20A roughness. A similar procedure was applied for the normalised vertical profiles of the stresses for the C20S, C10S and RM10S cases, shown in Figure 7–9 respectively, and the results

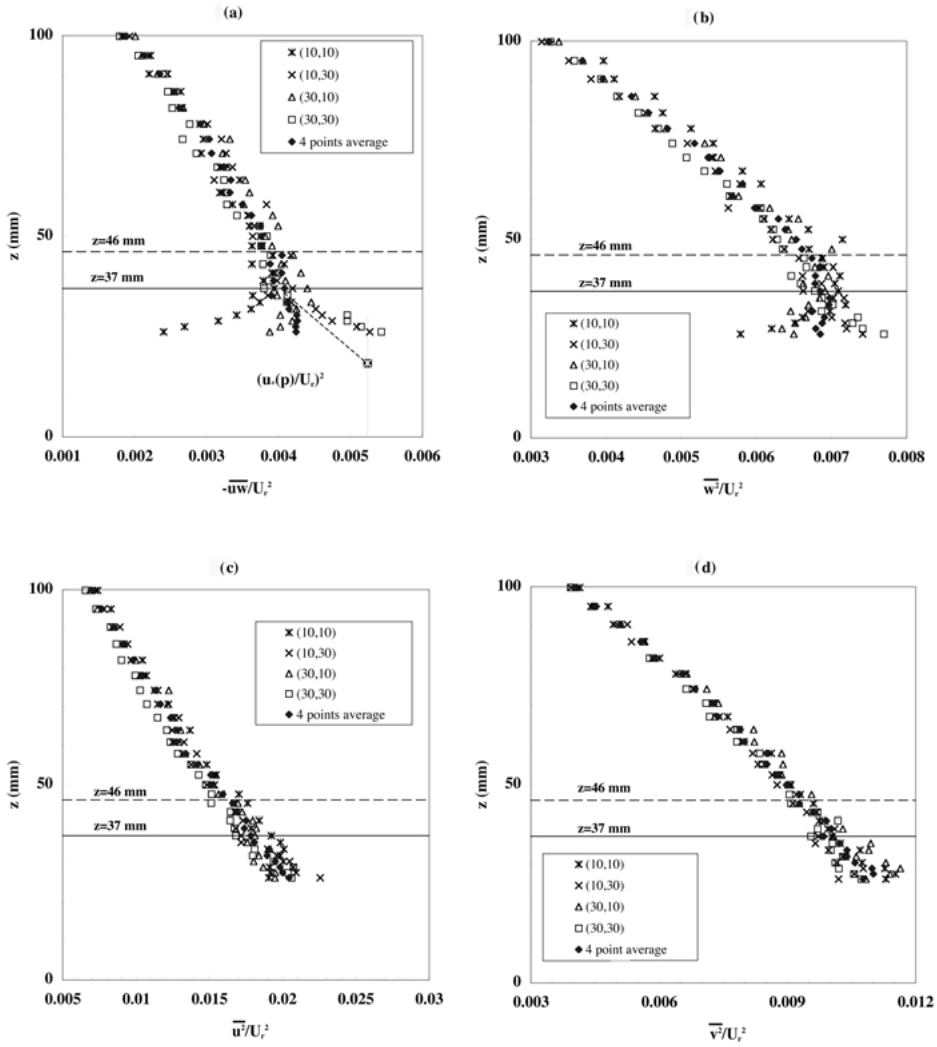

Figure 7. Vertical profiles over staggered cube arrays (C20S): (a) Shear stress; (b) vertical stress; (c) longitudinal stress; (d) lateral stress.

for all the roughnesses are listed in Table III. The number of data points in the IS and RS for each surface is also included in the last two columns of Table III.

Comparing the results for the aligned and staggered 20-mm cube array surfaces (C20A and C20S), it seems that the thicknesses of the IS and RS remain roughly the same for these two extreme wind directions. Note also that for the two staggered cube arrays (C20S and C10S), which are geometrically similar, the thicknesses of the RS appear to be a function of the height of the roughness elements (1.8–1.85h), as might be expected for fully developed conditions (which

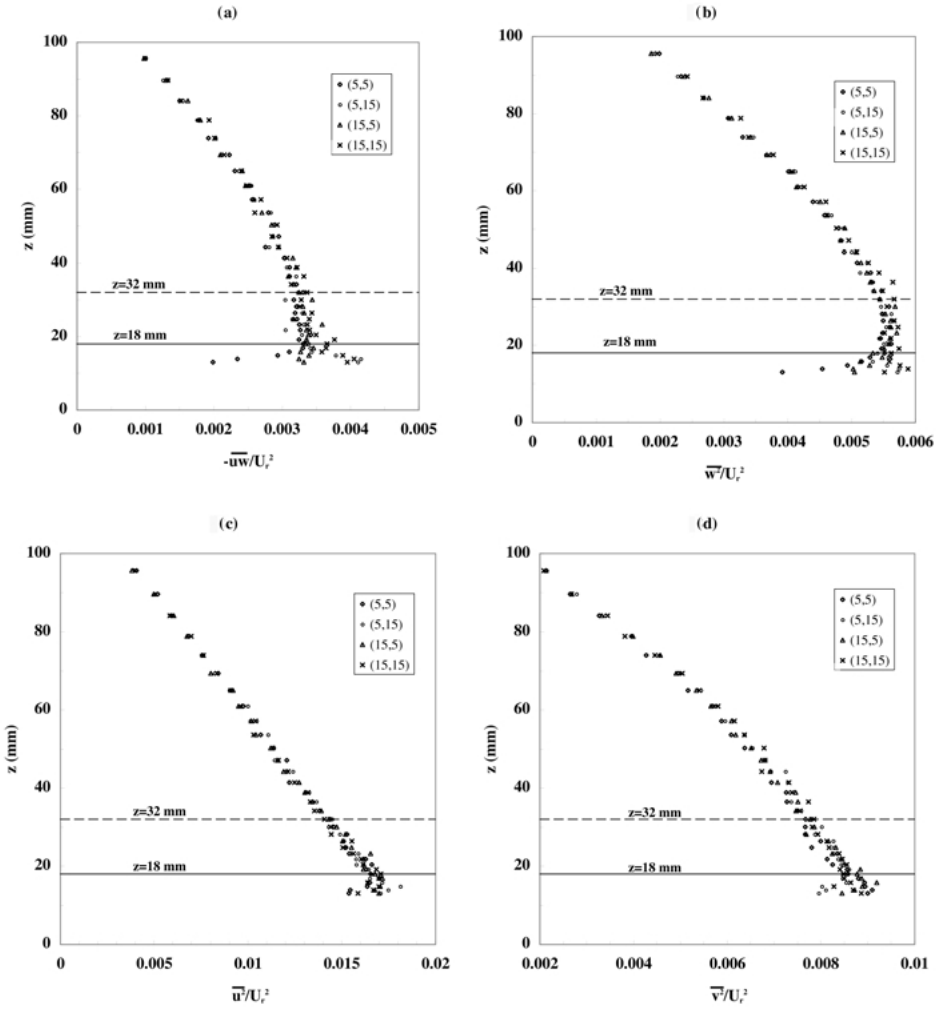

Figure 8. Vertical profiles over staggered cube arrays (C10S): (a) Shear stress; (b) vertical stress; (c) longitudinal stress; (d) lateral stress.

requires sufficient fetch, of course). Comparing C10S and RM10S, which have the same mean roughness height of 10 mm, the upper limits of the inertial sublayer are almost identical at similar fetch, but the inertial sublayer for the random surface is much thinner than that for the uniform one, not surprisingly, because of the intrusion of the taller elements into the RS. This implies that the inertial sublayer may not exist at all in urban areas where the dominant features are extremely high, irregular and heterogeneous roughness elements. It is clear that the random surface is rougher than the uniform one of the same (average) element height, and should be more effective for turbulent momentum transfer.

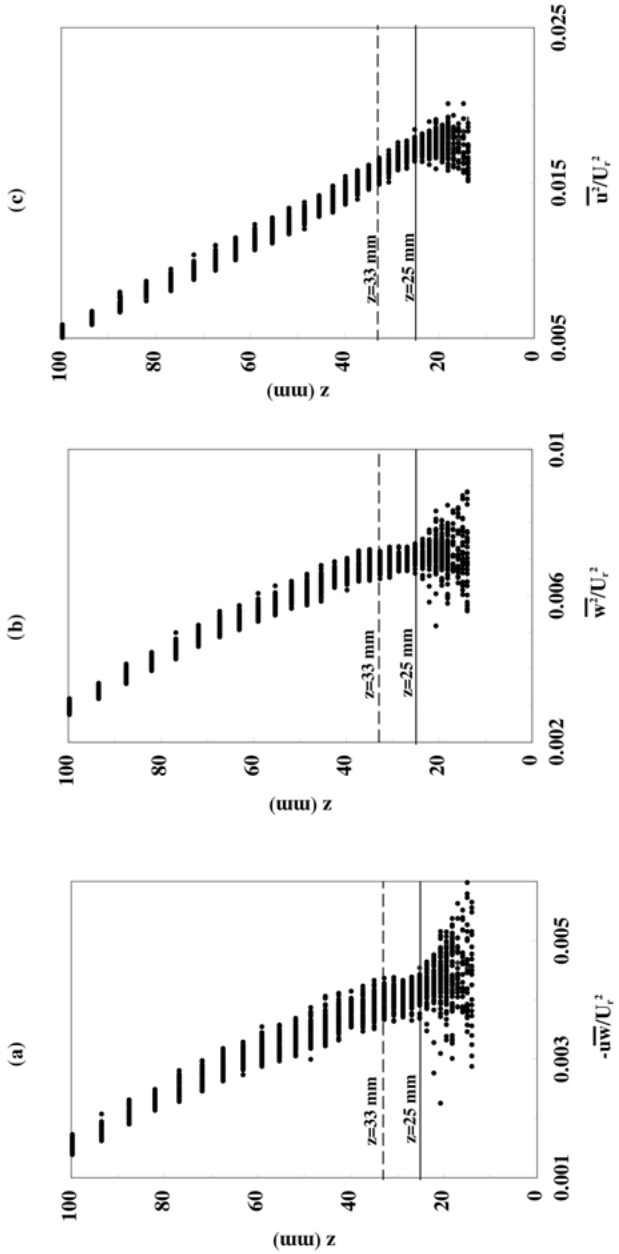

Figure 9. Vertical profiles over staggered random arrays (RM10S): (a) Shear stress; (b) vertical stress; (c) longitudinal lstress.

TABLE III
Various layer thicknesses over cube arrays.

Roughness	Instrumentation	x (mm)	δ (mm)	RS (mm) (data points)	IS (mm) (data points)
C20A	120° x-wire	2970	151	37 (7 points)	37–48 (7 points)
C20S	120° x-wire	2950	141	37 (10 points)	37–46 (7 points)
	LDA	3120	148	34 (5 points)	34–46 (7 points)
C10S	120° x-wire	3145	121	18 (10 points)	18–32 (10 points)
RM10S	120° x-wire	3125	136.5	25 (10points)	25–33 (4 points)

4.3. Spatially averaged data in the IS and RS

Based on the definition of u_* in Equation (1) the sensible value of u_* is $u_*(p)$, derived from the form drag of the surface (and assuming negligible viscous contribution). For the C20A roughness, this $u_*(p)$ was used as the slope to fit the 25-point-averaged mean velocity in both the RS and IS to the usual logarithmic law, as shown in Figure 10. This gave a zero-plane displacement of 16.7 mm and a roughness length of 0.95 mm for this aligned cube array roughness.

Usually, of course, it is not possible to measure the form drag directly, particularly for random surfaces, so that often u_* is estimated from turbulence shear stress measurements made above the surface. We denote the values deduced from the spatially averaged shear stresses in the IS, the RS or the whole surface layer (RS and IS together) by u_*(IS), u_*(RS), and u_*(IS&RS) respectively. Using these various u_* as slopes to best-fit the spatially averaged mean velocity in the corresponding layers yields different values of d and z_0; the resulting profiles are included in Figure 10. It is clear that the best fits occur when using a u_* either from the direct drag measurements or from the shear stress data averaged throughout the RS and the IS (u_*(IS&RS)) – i.e., spatially averaged within the RS, as well as vertically averaged. Note especially that using the IS shear stress data alone does not yield consistent results.

Alternatively, we could assume that the zero-plane displacement height is the effective height at which the surface drag acts (see, e.g., Jackson, 1981, for physical arguments supporting this idea). The pressure measurements on the roughness element then allow a direct determination of d. For the C20A roughness, the estimated $d' = 12.44$ mm (using a prime to differentiate this d from that derived from best fits to the mean velocity profile). Using $u_*(p)$ and d' to best-fit the spatially averaged mean velocity then gives $z_0' = 1.2$ mm. However, as shown in Figure 10, no log-law region then exists (unless one accepts a significantly different value for von Karman's constant). This is possibly a valid conclusion, but given the general ubiquitous and forgiving nature of the log-law, it seems more likely that, unlike dense forest-like roughnesses (Thom, 1971; Jackson, 1981), the displacement height for

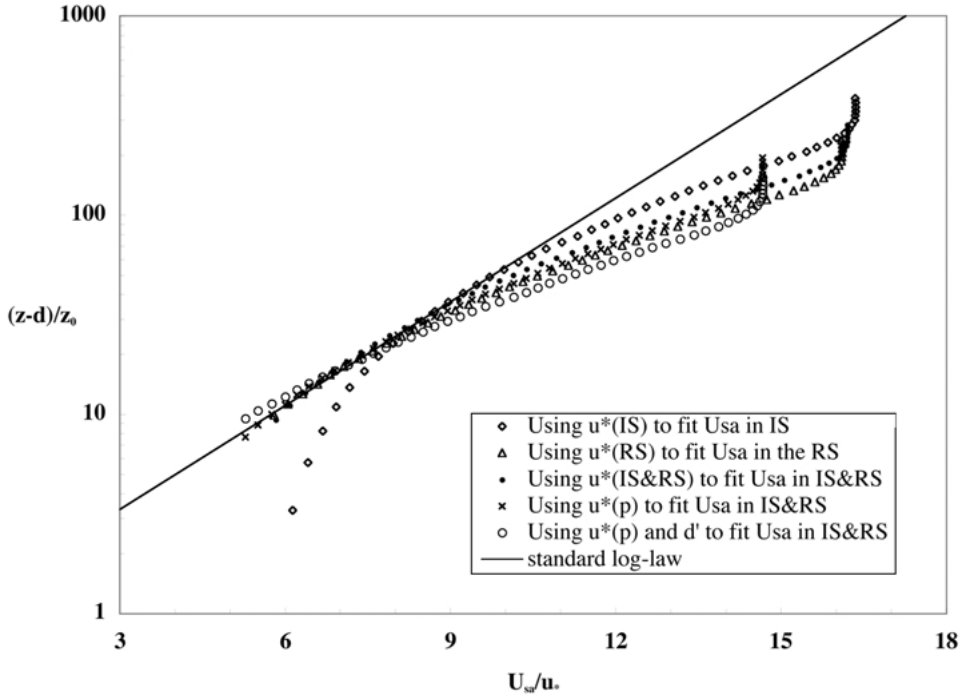

Figure 10. Spatially averaged mean velocity over C20A surface.

an urban surface is actually not coincident with the centre at which the element form drag acts. This may imply that the dispersive stresses within the urban canopy layer are significant, which is certainly likely but is in contrast to what has been observed in the RS (see Section 4.5). The corresponding results for C20S are shown in Figure 11, where $d' = 12.17$ mm and $z_0' = 1.5$ mm, and similar conclusions apply to that case. Figure 12 shows data for C10S and RM10S, limited in this case to the surface layer only. Form drag measurements were not conducted on the C10S and RM10S surfaces. The surface properties for all the surfaces at similar fetch are summarised in Table IV.

In all these cases use of u_* (IS&RS) (or $u_*(p)$ when available) gave the best results and the spatially averaged mean velocity profiles normalised by the individual u_* (IS&RS) for all the surfaces studied here are shown in Figure 13. The results in Figures 10–13 emphasise the point made by Ploss et al. (2000) that, by spatially averaging over a repeat unit, the logarithmic region can be extended to the roughness sublayer. This disagrees with the conclusion draw by Raupach et al. (1986), who found that the averaged velocity profile in the RS over a plant canopy was not logarithmic with any sensible choice of d. The different conclusions for urban-like and forest-like surfaces may imply that the flow in the RS behaves differently over these two different kinds of surfaces.

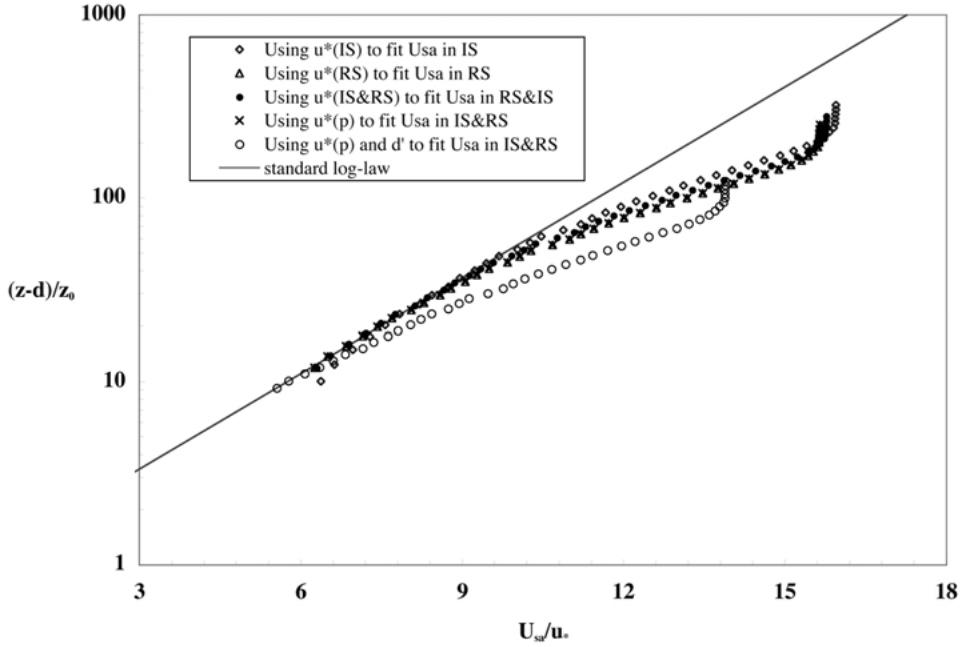

Figure 11. Spatially averaged mean velocity over C20S surface.

Comparing results from the C20A and C20S surfaces, it is seen that the surface friction velocity $u_*(p)$ derived from the form drag measurements by neglecting viscous effects is significantly higher than the various u_* obtained from the direct shear stress measurements using x-wire anemometry (or, indeed, the LDA). Since this conclusion is true for both x-wire and LDA data it is difficult to believe that the difference is entirely due to experimental errors and the evidence suggests that the shear stress in the IS is indeed somewhat lower than the surface stress. In fact, the surface stress values are not too far from what might be deduced by a linear extrapolation of the measured $\overline{uw}$ from their (averaged) values, although this is less true for the staggered array (Figure 7a). $u_*(p)$ data for C20A and C20S are included in Figures 6a and 7a at a vertical height of $z = d$ (which would seem more appropriate than $z = 0$). Use of $u_*(p)$ also gives more physically reasonable values for d than are obtained using u_* (IS) (see below); note that use of u_* (IS) is common practice for determination of roughness length in wind-tunnel simulations of the atmospheric boundary layer. From the best-fit point of view, using u_* (IS&RS) gives a similar standard error as using $u_*(p)$, but yields a z_0 value some 35% lower. Examining the data listed in Table IV, for all the roughnesses involved in this investigation, the displacement heights interpreted from the shear stress measurements in the inertial sublayer alone are close to the building height itself, which does not seem to be physically sensible. These results also suggest that the conventional way of determining the roughness length, using u_* derived from

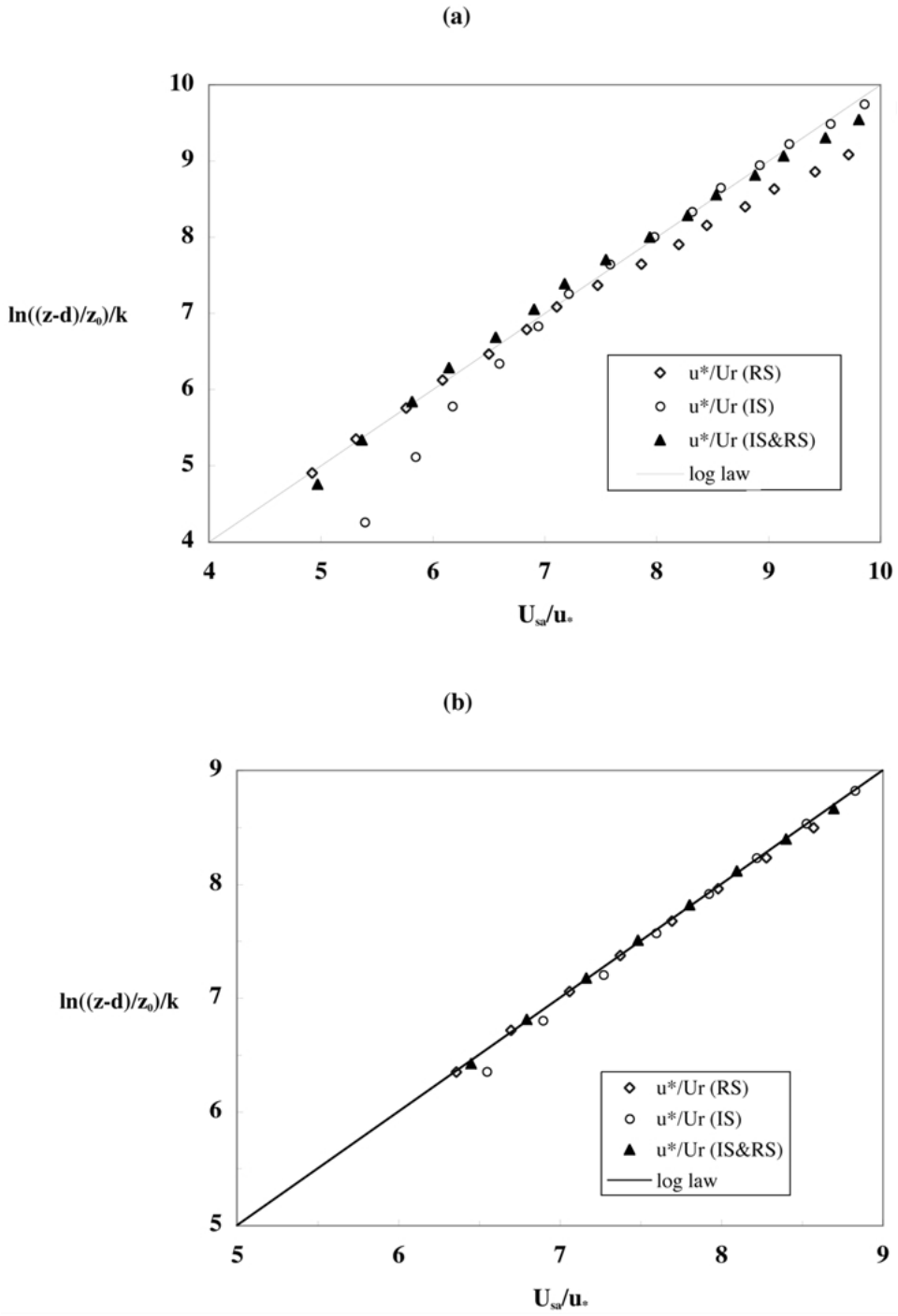

Figure 12. Spatially averaged mean velocity over roughnesses of (a) C10S, (b) RM10S.

TABLE IV
Surface characteristics for all roughness arrays.

		$u_*/U_r(p)$	u_*/U_r (IS&RS)	u_*/U_r (IS)	u_*/U_r (RS)
C20A	u_*/U_r	0.0679	0.0614	0.0609	0.0618
	d (mm)	16.7	18.0	23.5	16.4
	z_0 (mm)	0.95	0.64	0.46	0.77
	$u_*/u_*(p)$	1.00	0.91	0.90	0.91
C20S	u_*/U_r	0.0724	0.0638	0.0631	0.0643
	d (mm)	16.6	18.4	20.6	17.5
	z_0 (mm)	1.07	0.65	0.56	0.73
	$u_*/u_*(p)$	1.00	0.88	0.87	0.89
C20S	u_*/U_r	0.0724	0.0635	0.0631	0.0639
by LDA	d (mm)	14.5	16.7	19.5	14.8
	z_0 (mm)	1.33	0.81	0.69	0.95
	$u_*/u_*(p)$	1.00	0.88	0.87	0.88
C10S	u_*/U_r		0.0579	0.0577	0.0585
	d (mm)		9.7	11.6	8.6
	z_0 (mm)		0.49	0.41	0.62
RM10S	u_*/U_r		0.0644	0.0634	0.0653
	d (mm)		12.4	13.6	11.9
	z_0 (mm)		0.64	0.56	0.70
		IS&RS	IS&RS	in IS	in RS

the vertical profile taken in the inertial sublayer, would significantly under-estimate the roughness length z_0.

The results from both the form drag measurements and direct shear stress measurements have confirmed that the staggered arrays experience a higher overall drag force and provide a greater resistance to the flow than the aligned arrays (some 14% on wall stress), due no doubt to the greater exposure of the roughness elements to the flow. This agrees well with the conclusion drawn by Macdonald et al. (2000) for higher packing density, but it is quantitatively inconsistent with the claim made by Grimmond and Oke (1999) that the roughness length for a staggered array is twice as large as it is for an equivalent in-line array. Note also that the difference in the ratio of u_* to $u_*(p)$ listed in Table IV for C20A and C20S is consistent with the idea that viscous drag may not be entirely negligible for the aligned array (or at least less negligible than for the staggered array). This seems intuitively quite possible. The difference in u_*/U_r for the geometrically identical C20S and C10S arrays is simply a result of fetch – see Section 4.4.

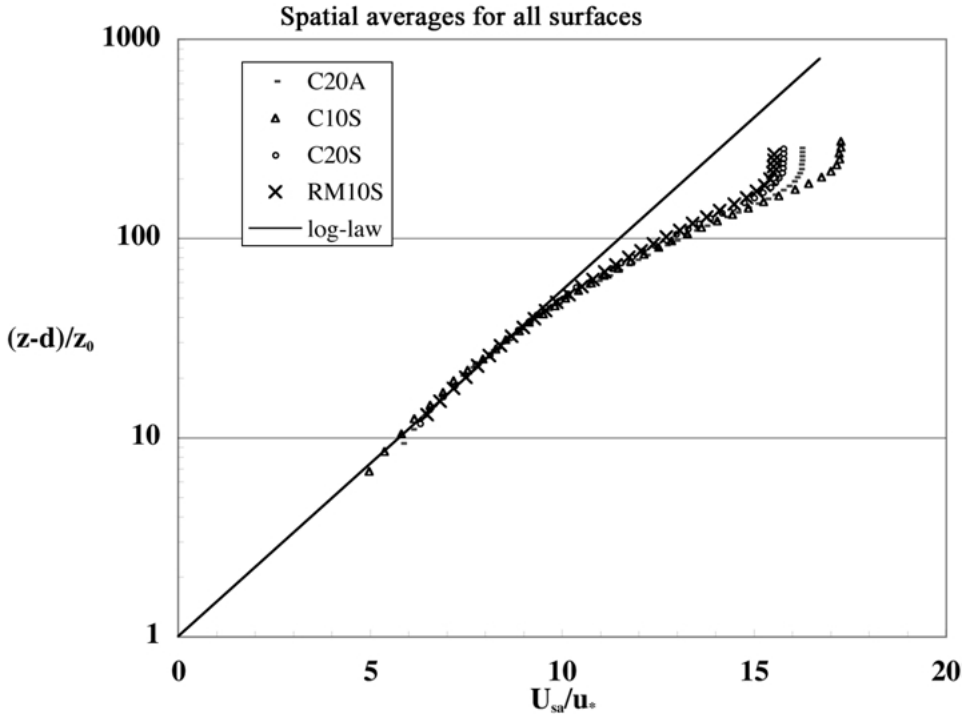

Figure 13. Spatially averaged mean velocity normalised by u_* (IS&RS) for all surfaces.

Some recent studies (Macdonald, 2000; Plate, 1995; Grimmond and Oke, 1999; Raupach et al., 1991) have indicated that the displacement height d and the roughness length z_0 measured in cities are primarily functions of plan area density and frontal area density respectively. (Frontal area density is usually defined as the ratio of the total frontal area of the obstacles in a repeating unit to the plan area of that unit). Table IV shows that despite the significant difference in surface stress between staggered and aligned arrays (C20S and C20A), the values of d/h and z_0/h are both very similar in the two cases and are also close to those for the C10S array (recall that small differences in u_* lead to much larger changes in z_0, so that the difference in z_0/h between the C10S and C20S cases is probably within the level of uncertainty). Now both the plan area density and the frontal area density are identical in these three cases so these results are not inconsistent with the earlier studies. An alternative (perhaps more intuitive) definition of frontal area density would be the ratio of total element frontal area in a repeating unit to the total 'envelope' area given by the average height of the elements multiplied by the spanwise width of the repeating unit. This is 50% for the aligned arrays and 100% for the staggered arrays in the present cube cases. It would seem that this difference is insufficient to generate, on its own, very significant changes in d and z_0. The values of the roughness length and friction velocity for C10S and RM10S also confirm

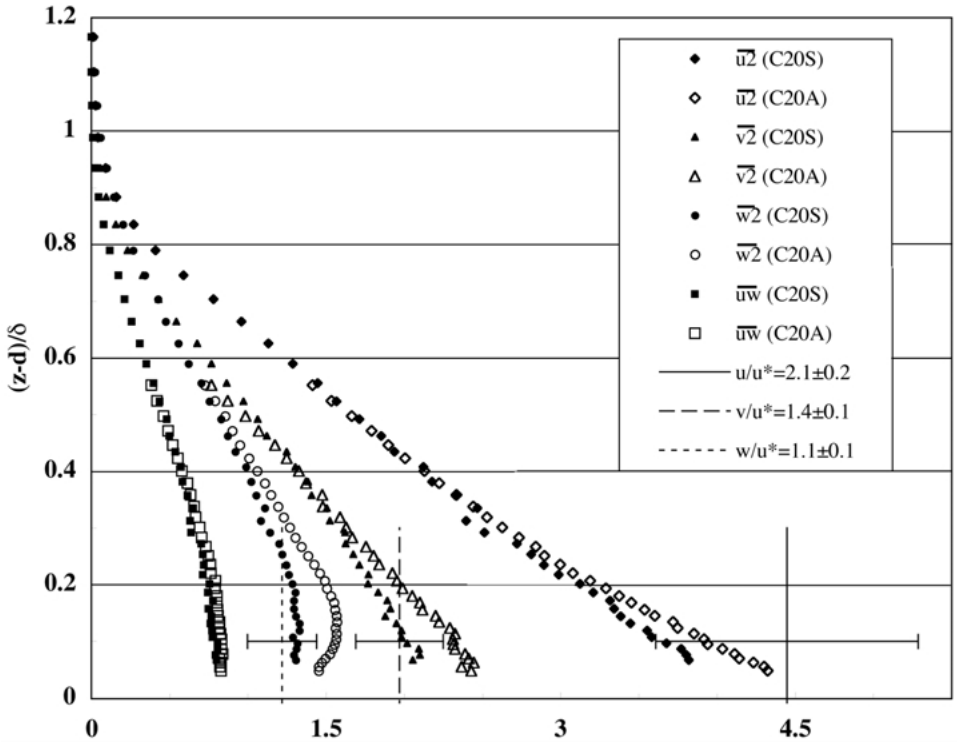

Figure 14. Spatially averaged stresses for C20A and C20S surfaces.

the statement made by Grimmond and Oke (1999), that an array of elements with uniform heights is less rough than one with variable heights, even though they have the same plan and (standard) frontal area density as well as mean height. This also indicates that the roughness length is dependent on the standard deviation of height variability in roughness elements, which seems entirely reasonable.

For the C20A and C20S roughnesses the vertical profiles of spatially averaged stresses normalised by $u_*(p)$ are plotted against $(z-d)/\delta$ in Figure 14. These results are compared with data at $(z-d)/\delta = 0.1$ from both smooth and rough wall boundary layers obtained by Raupach et al. (1991), also shown in Figure 14. The agreement is reasonable, particularly in view of the uncertainties in the latter, but the data do indicate small differences between the two roughness arrangements. The spatially averaged stresses normalised by u_* (IS&RS) for all the staggered roughnesses at similar fetch are compared in Figure 15. There is a reasonable collapse, apart from small (but measurable) differences in the longitudinal component.

The spatially averaged correlation coefficient ($r_{uw} = \overline{uw}/(\sqrt{\overline{u^2}}\sqrt{\overline{w^2}})$) in the surface layer for all the roughnesses is shown in Figure 16. For C20S and C10S the data are almost identical, but obvious differences exist between different surface

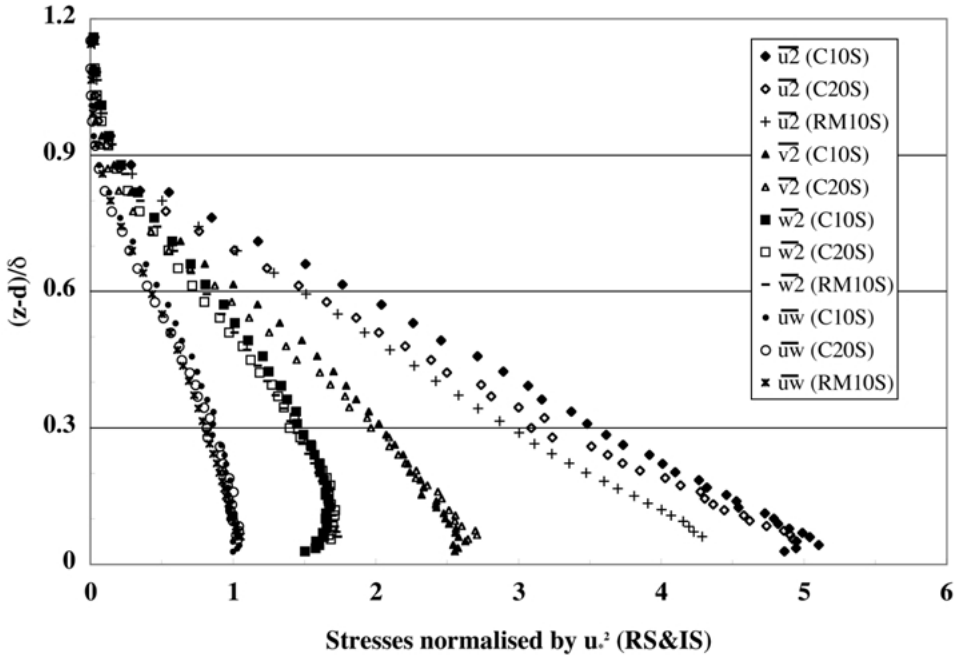

Figure 15. Spatially averaged stresses for staggered surfaces at similar fetch (C20S, C10S and RM10S).

types. Comparing the C20S and RM10S surfaces, which have almost identical u_*/U_r, z_0 and δ, the correlation coefficients in the surface layer for RM10S are some 9% higher than for the C20S surface, indicating an increased 'turbulence efficiency' in generation of shear stress. Nevertheless, the correlation coefficients for all the roughnesses studied here are in the range 0.36 ± 0.03.

4.4. The effects of fetch

To study the effects of fetch on the development of the roughness sublayer and inertial sublayer, in addition to the measurements at $x = 3145$ mm over the C10S surface, corresponding data were obtained at various longitudinal locations at the same nominal free stream velocity of 10 m s^{-1}. At each fetch, using the procedures discussed in Sections 4.1 and 4.2, four vertical profiles uniformly distributed in a unit area were taken and these profiles were examined so that the depths of the RS and IS at that location could be determined. The growth rates of various layers with fetch over the C10S surface are shown in Figure 17. These data clearly demonstrate that the thickness of the roughness sublayer is essentially independent of fetch after an initial (short) development region. The depth of the IS increases with fetch, as expected, although not as rapidly as the boundary-layer depth, whilst the ratio of the height corresponding to the top of the IS to the thickness of the boundary-layer at each location, shown in Figure 18, decreases significantly with fetch –

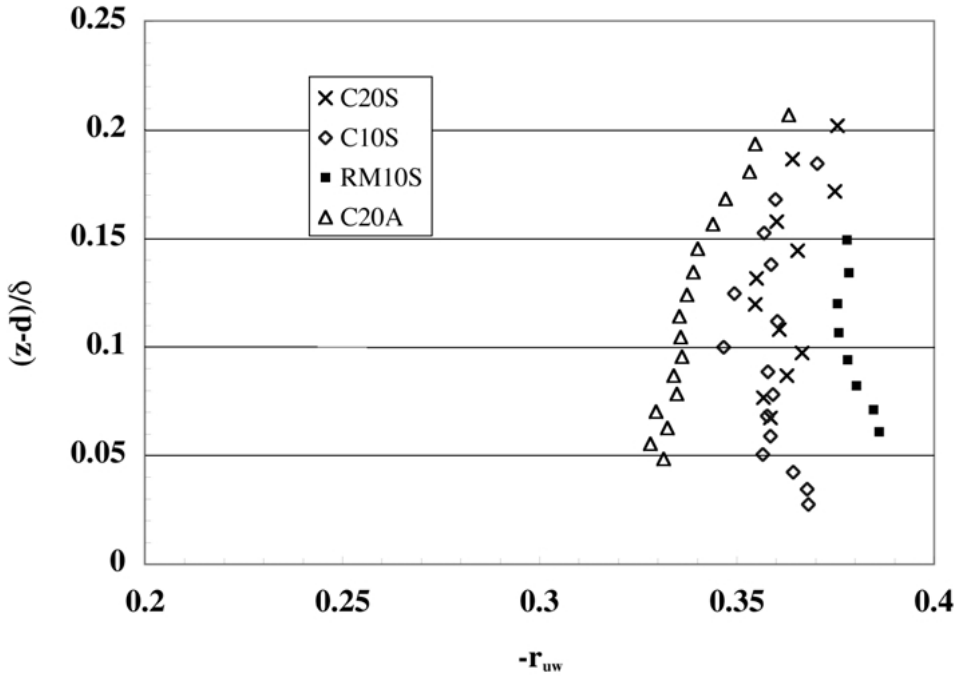

Figure 16. Spatially averaged correlation coefficient for all surfaces.

plotted here non- dimensionally as δ/h – and approaches the generally accepted value of 0.25δ as quoted by Macdonald (2000). Note that for most of the fetch the boundary-layer growth is closely linear (Figure 17).

Constant $d\delta/dx$ is one of the requirements for a self-preserving boundary layer (see Smalley et al., 2001, for a recent useful discussion); the other more stringent requirement is that the skin friction C_f (where $C_f = 2(u_*/U_r)^2$) should be constant with fetch but the data shown in Figure 19 indicate that it is not. The C10S flow is thus not genuinely self-preserving, although the variation of surface stress is weaker than it would be for a smooth wall boundary layer over the same Reynolds number range. The u_* values derived from the spatially averaged shear stress in the RS and IS and also the values deduced from the shear stress at z = 18 mm (which is the border between the RS and the IS for the C10S surface) are included in Figure 19a, again as a function of δ/h to facilitate comparison with the data for the other surfaces. As noted above, there is a slow but steady fall in u_* with fetch. The roughness length obtained by fitting the spatially averaged mean velocity to the standard log-law using u_* (IS&RS) is shown in Figure 19b. It is clear that z_0 increases with fetch up to around x = 1.5 m where δ/h = 6.9, while the canopy layer and roughness sublayers are developing, but then remains roughly constant. Figures 18 and 19 include corresponding data for the other surfaces (at the one location used); these collapse reasonably well as anticipated.

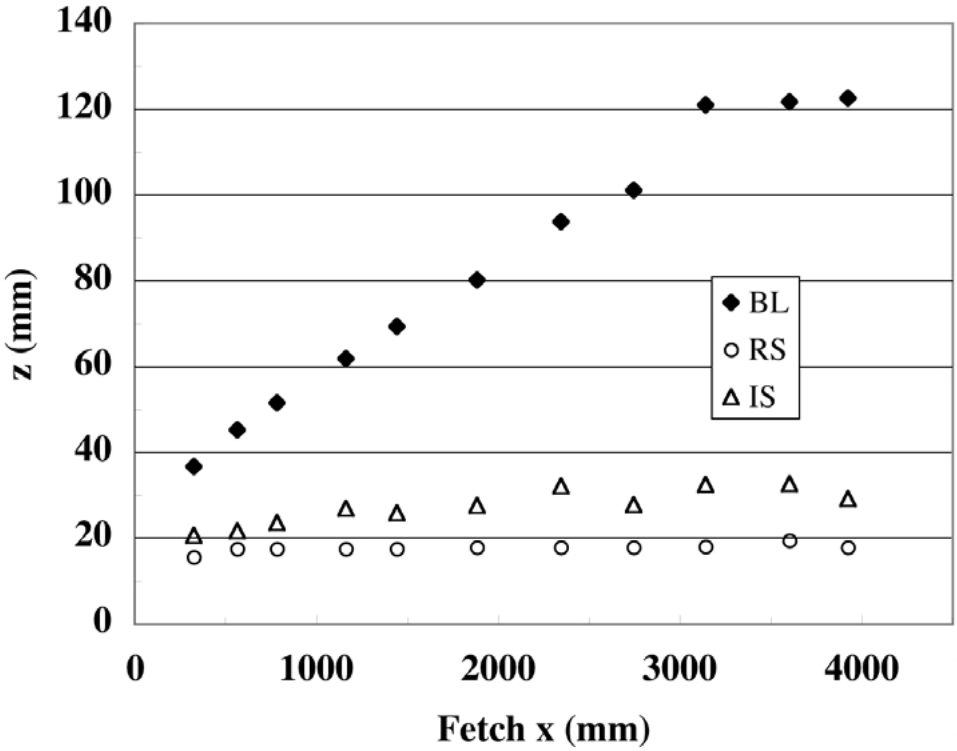

Figure 17. Development of various layers over C10S roughness. BL, RS and IS refer to the depths of the boundary layer, the top of the roughness sublayer and the top of the inertial layer, respectively.

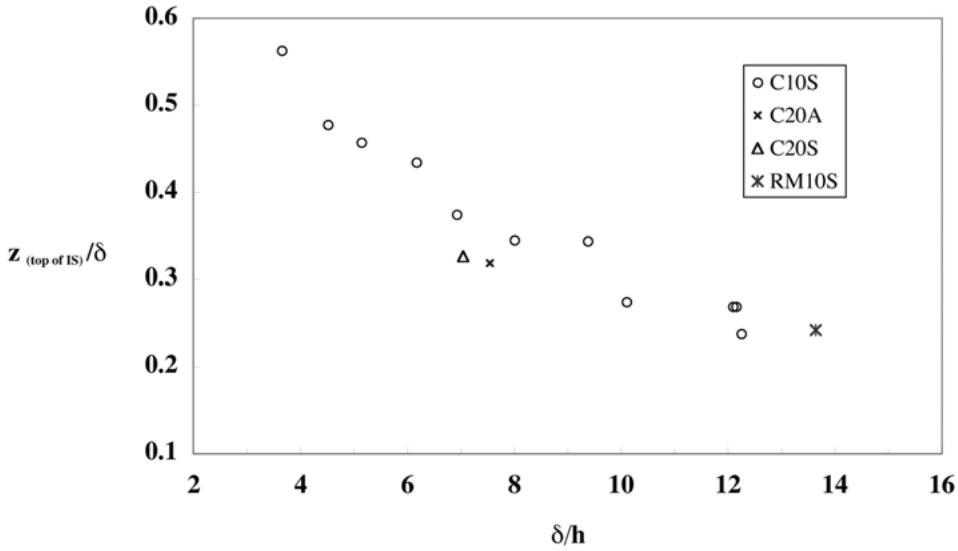

Figure 18. Growth of the surface layer with fetch.

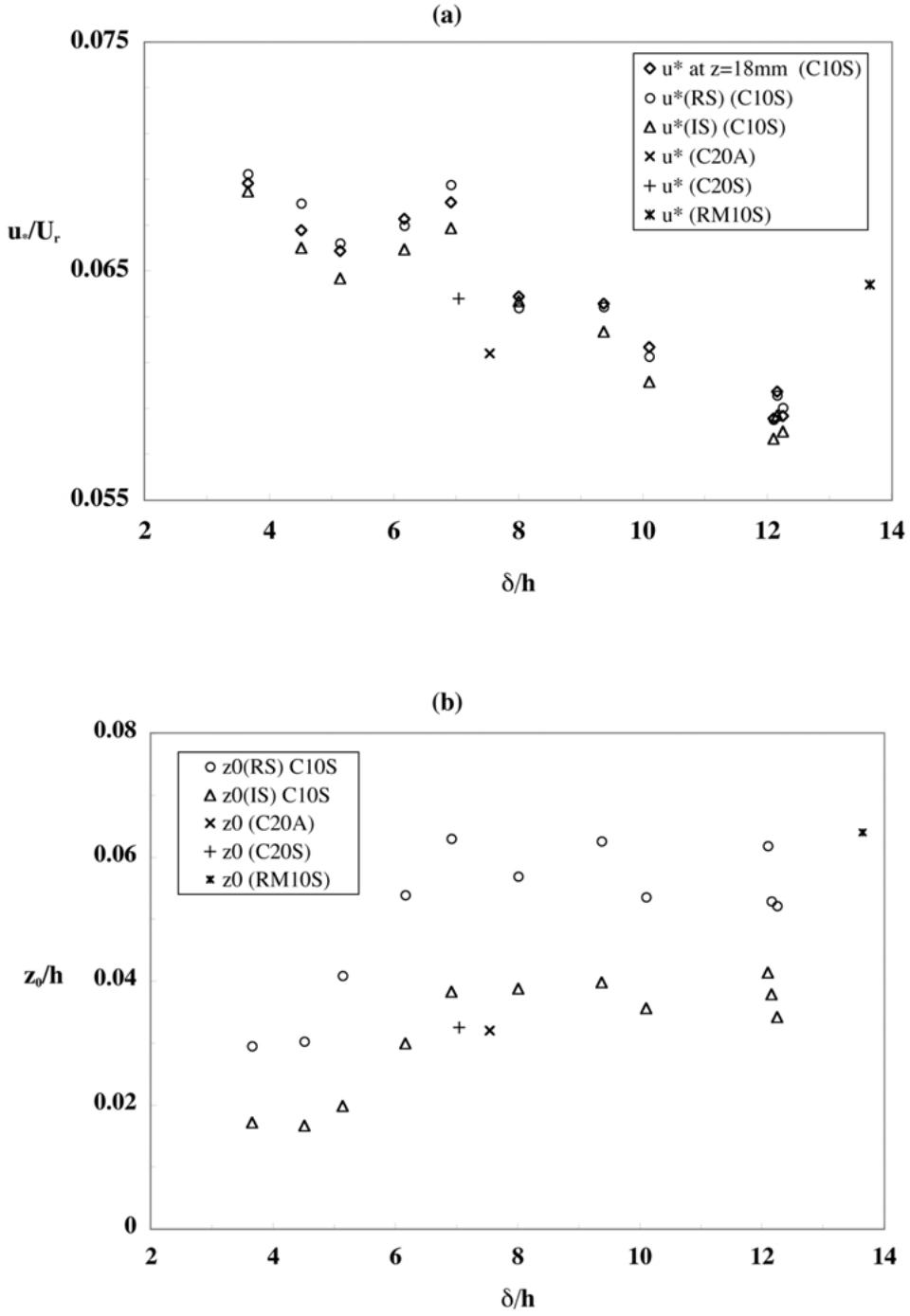

Figure 19. Development of u_* (a) and z_0 (b) with fetch over C10S surface. Note the false origin in (a).

4.5. Dispersive stress in the RS over C20A and RM10S roughness

In the roughness sublayer the flow is inherently three dimensional. At the same height, the time averaged mean flow velocities at different locations within a repeating unit are usually different, which results in additional momentum transfer within the horizontal plane. Dispersive stresses represent the contribution to momentum transfer from correlations between point-to-point variations in the time-averaged flow. Denoting them by angular brackets they can be defined as follows:

$$\langle \overline{u^2} \rangle = \frac{1}{n} \sum_{i=1}^{n} (\bar{U}_i - \bar{U}_{sa})^2, \tag{4a}$$

$$\langle \overline{w^2} \rangle = \frac{1}{n} \sum_{i=1}^{n} (\bar{W}_i - \bar{W}_{sa})^2, \tag{4b}$$

$$\langle \overline{uw} \rangle = \frac{1}{n} \sum_{i=1}^{n} (\bar{U}_i - \bar{U}_{sa})(\bar{W}_i - \bar{W}_{sa}). \tag{4c}$$

These stresses have been deduced for the C20A and RM10S surfaces, as only in these cases was a sufficient number of vertical profiles taken (n = 25 and 64, respectively) to enable Equation (4) to yield reasonable averages. The results are shown in Figures 20 and 21. Note that the non-zero values above the RS must indicate the degree of experimental uncertainty. Nonetheless, compared with the spatially averaged Reynolds stresses, the dispersive stresses are clearly negligible in the range of $z > h$ for urban roughness. This is consistent with the conclusion drawn from flow over plant canopies by Raupach et al. (1986) and Böhm et al. (2000) although in the canopy layer ($z < h$) Böhm et al. demonstrate that the dispersive flux can be significant compared with the normal turbulent fluxes. Whether this would be true also for urban-type roughness of the kind used here remains an open question and requires very extensive and technically difficult measurements before a conclusive answer is possible.

5. Conclusions

Comprehensive measurements in a repeating unit over a number of urban roughnesses (all having 25% plan and frontal area density) have demonstrated the three dimensionality of the flow in the roughness sublayer (RS). The depths of the RS are found to be independent of both wind direction and (after the initial development region) fetch. For cube arrays, the depth of the RS is 1.8–1.85h, where h is the cube height. Staggered cube arrays provide greater drag to the flow than the aligned cube arrays at the same flow conditions. The spatially averaged mean velocity in

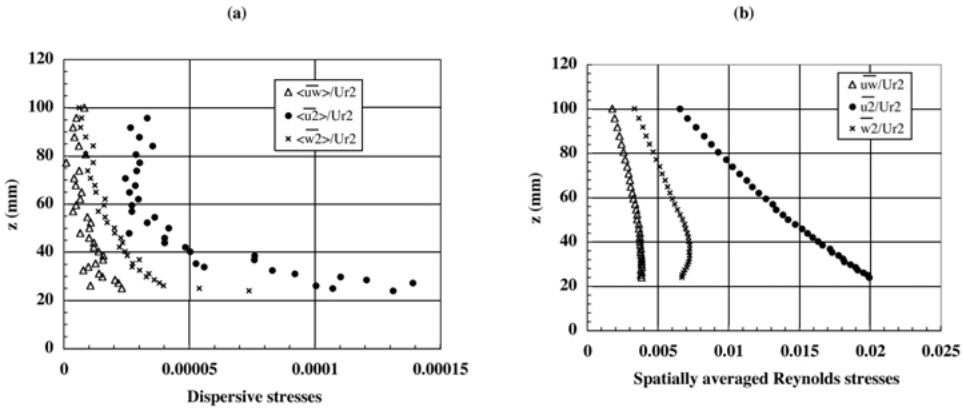

Figure 20. Comparison between dispersive stresses and Reynolds stresses over C20A surface.

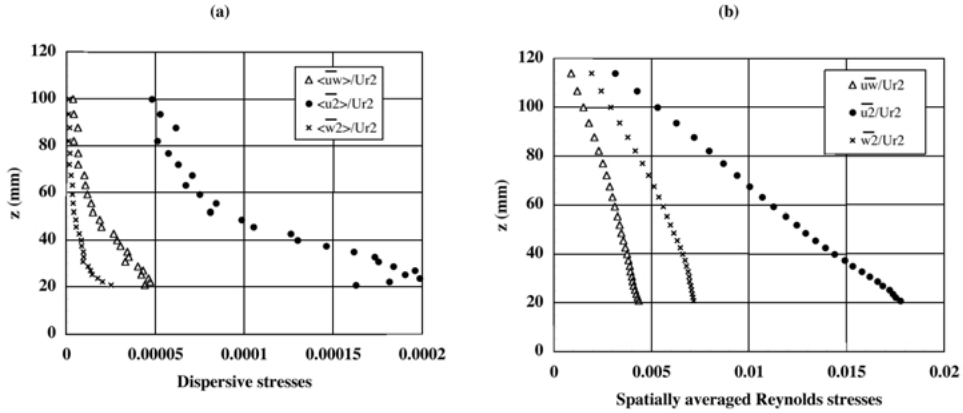

Figure 21. Comparison between dispersive stresses and Reynolds stresses over RM10S surface.

the roughness sublayer and inertial sublayer can (together) be described by a single log-law, provided an appropriate u_* for the surface is known. This is best obtained by techniques more direct than either *assuming* the presence of a log-law region and deducing u_* from measured shear stresses or from mean flow profiles, or taking it from spatially averaged shear stress measurements within the roughness sublayer; the latter does, however, provide more self-consistent results than the former. Using data from the log-law region only (if it exists) does *not* give the correct surface parameters. This study seems to suggest that the flow over urban canopies and plant canopies is different.

The dispersive stresses arising from the inhomogeneity in the mean flow in the RS are shown to be negligible compared with the spatially averaged Reynolds stresses. A random height roughness of the same plan arrangement and total volume as a regular array is more efficient at generating surface stress. Furthermore, although the upper limits of the inertial sublayer for both surfaces are almost identical, the roughness sublayer is much thicker for the random surface than for

the uniform surface. This increases the likelihood that an inertial sublayer may not exist at all in some urban areas in which the dominant features are high, irregular and heterogeneous roughness elements. Similar experiments with further 'randomisation' of the surface (e.g., random positioning as well as random heights) would be useful in assessing the extent to which the present conclusions are valid for arbitrary surfaces.

Acknowledgements

We thank Paul Hayden, Allan Wells and Tom Lawton in the EnFlo laboratory for their technical help. This project is funded by the Natural Environment Research Council through Grant GST/04/2231 under the URGENT programme and through the UWERN urban meteorology programme; their financial support is gratefully acknowledged. We would also like to thank the referees for careful reading of the manuscript and some helpful comments.

References

Böhm, M., Finnigan, J. J., and Raupach, M. R.: 2000, 'Dispersive Fluxes and Canopy Flows: Just how Important Are They?', in *American Meteorology Society, 24th Conference on Agricultural and Forest Meteorology*, 14–18 August 2000, University of California, Davis, CA, pp. 106–107.

Cheng, H. and Castro, I.: 2002, 'Near-Wall Flow Development after a Step Change in Surface Roughness', *Boundary-Layer Meteorol.*, in press.

Garratt, J. R.: 1980, 'Surface Influence upon Vertical Profiles in the Atmospheric Near-Surface Layer', *Quart. J. Roy. Meteorol. Soc.* **106**, 803–819.

Grimmond, C. S. B. and Oke, T. R.: 1999, 'Aerodynamics Properties of Urban Areas Derived from Analysis of Surface Form', *J. Appl. Meteorol.* **38**, 1262–1292.

Jackson, P. S.: 1981, 'On the Displacement Height in the Logarithmic Velocity Profile', *J. Fluid Mech.* **111**, 15–25

Kaimal, J. C. and Finnigan, J. J.: 1994, *Atmospheric Boundary Layer Flows: Their Structure and Measurement*, Oxford University Press, ISBN 0-19-506239-6.

Macdonald, R. W.: 2000, 'Modelling the Mean Velocity Profile in the Urban Canopy Layer', *Boundary-Layer Meteorol.* **97**, 25–45.

Macdonald, R. W., Carter, S., and Slawson, P. R.: 2000, *Measurements of Mean Velocity and Turbulence Statistics in Simple Obstacle Arrays at 1:200 Scale*, Thermal Fluids Report 2000-1, University of Waterloo, Canada.

Modi, V. J. and Deshpande, V. S.: 2001, 'Fluid Dynamics of a Cubic Structure as Affected by Momentum Injection and Height', *J. Wind Eng. And Ind. Aero.* **89**, 445–470.

Mulhearn, P. J. and Finnigan, J. J.: 1978, 'Turbulent Flow over a Very Rough, Random Surface', *Boundary-Layer Meteorol.* **15**, 109–132.

Perry, A. E., Henbest, S., and Chong, M. S.: 1986, 'A Theoretical and Experimental Study of Wall Turbulence', *J. Fluid Mech.* **165**, 163–199.

Perry, A. E., Lim, K. L., and Henbest, S. M.: 1987, 'An Experimental Study of the Turbulence Structure in Smooth and Rough Wall Turbulent Boundary Layer', *J. Fluid Mech.* **177**, 437–466.

Plate, E. J.: 1995, 'Urban Climates and Urban Climate Modelling: An Introduction', in J. E. Cermak et al. (eds.), *Wind Climate in Cities*, Kluwer Academic Publishers, Dordrecht, Boston, pp. 23–39.

Plate, E. J. (ed.): 1982, *Engineering Meteorology: Studies in Wind Engineering and Industrial Aerodynamics*, Vol. 1, Elsevier Scientific Publishing Company, Amsterdam, New York.

Ploss, A., Castro, I., and Cheng. H.: 2000, 'The Surface Region of Rough-Wall Boundary Layers', in C. Dopazo (ed.), *Advances in Turbulence VIII*, CIMNE, pp. 455–459.

Ranga Raju, K. G., Loeser, J., and Plate, E. J.: 1976, 'Velocity Profiles and Fence Drag for a Turbulent Boundary Layer along Smooth and Rough Flat Plates', *J. Fluid Mech.* **76**, 383–399.

Raupach, M. R., Antonia, R. A., and Rajagopalan, S.: 1991, 'Rough-Wall Turbulent Boundary Layers', *Appl. Mech, Rev.* **44**, 1–25.

Raupach, M. R., Coppin, P. A., and Legg, B. J.: 1986, 'Experiments on Scalar Dispersion within a Model Plant Canopy Part I: The Turbulence Structure', *Boundary-Layer Meteorol.* **35**, 21–52.

Raupach M. R., Finnigan, J. J., and Brunet, Y.: 1996, 'Coherent Eddies and Turbulence in Vegetation Canopies: The Mixing – Layer Analogy', *Boundary-Layer Meteorol.* **78**, 351–382.

Raupach, M. R., Thom, A. S., and Edwards, I.: 1980, 'A Wind Tunnel Study of Turbulent Flow Close to Regularly Arrayed Rough Surfaces', *Boundary-Layer Meteorol.* **18**, 373–397.

Rotach, M. W.: 1993a, 'Turbulence Close to a Rough Urban Surface, Part I: Reynolds Stress', *Boundary-Layer Meteorol.* **65**, 1–28.

Rotach, M. W.: 1993b, 'Turbulence Close to a Rough Urban Surface, Part II: Variances and Gradients', *Boundary-Layer Meteorol.* **66**, 75–92.

Rotach, M. W.: 1995, 'Profiles of Turbulence Statistics above an Urban Street Canyon', *Atmos. Environ.* **29**, 1473–1486.

Roth, M.: 2000, 'Review of Atmospheric Turbulence over Cities', *Quart. J. Roy. Meteorol. Soc.* **146**, 941–990.

Roth, M. and Oke, T. R.: 1993, 'Turbulent Transfer Relationships over an Urban Surface. I: Spectral Characteristics', *Quart. J. Roy. Meteorol. Soc.* **119**, 1071–1104.

Smalley, R. J., Anotnia, R. A., and Djenidi, L.: 2001, 'Self-Preservation of Rough-Wall Turbulent Boundary Layer', *Eur. J. Mech. B(Fluids)* **20**, 591–602.

Snyder, W. H. and Castro, I. P.: 2002, 'The Critical Reynolds Number for Rough-Wall Boundary Layers', *J. Wind Eng. Ind. Aero.* **90**, 41–54.

Stull, R. B.: 1988, *An Introduction to Boundary Layer Meteorology*, Kluwer Academic Publishers, Dordrecht, 666 pp.

Thom, A. S.: 1971, 'Momentum Absorption by Vegetation', *Quart. J. Roy. Meteorol. Soc.* **97**, 414–428.

Tutu, N. K. and Chevray R.: 1975, 'Cross-Wire Anemometry in High Intensity Turbulence', *J. Fluid Mech.* **71**, 785–800.

Wood, N. and Mason, P.: 1993, 'The Pressure Force Induced by Neutral Turbulent Flow over Hills', *Quart. J. Roy. Meteorol. Soc.* **119**, 1233–1267.